

ARTICLE



Anastasis confers ovarian cancer cells increased malignancy through elevated p38 MAPK activation

Lili Sun¹, Chen Yao¹, Xiaojiao Li², Yuxing Wang², Ru Wang², Molin Wang², Qiao Liu², Denise J. Montell³, Changshun Shao⁴, Yaoqin Gong² and Gongping Sun¹✉

© The Author(s), under exclusive licence to ADMC Associazione Differenziamento e Morte Cellulare 2022

Activation of executioner caspases was once considered as a point of no return in apoptosis. However, in recent years, accumulating evidence has demonstrated that cells can survive executioner caspase activation in response to apoptotic stimuli through a process called anastasis. In this study, we developed a reporter system, mCasExpress, to track mammalian cells that survive executioner caspase activation. We demonstrate that anastatic ovarian cancer cells acquire enhanced migration following their transient exposure to apoptotic stimulus TRAIL or Paclitaxel. Moreover, anastatic cancer cells secrete more pro-angiogenic factors that enable tumor angiogenesis, growth and metastasis. Mechanistically, we demonstrate that activation of p38 MAPK, which occurs in a caspase-dependent manner in response to apoptotic stress to promote anastasis, persists at a higher level in anastatic cancer cells even after removal of apoptotic stimuli. Importantly, p38 is essential for the elevated migratory and angiogenic capacity in the anastatic cells. Our work unveils anastasis as a potential driver of tumor angiogenesis and metastasis.

Cell Death & Differentiation (2023) 30:809–824; <https://doi.org/10.1038/s41418-022-01081-1>

INTRODUCTION

Apoptosis is a conserved cell suicide process that functions to remove excess or damaged cells during development or when encountering stress. Apoptosis is typically initiated by interaction between death receptors and their ligands or mitochondrial outer membrane permeabilization (MOMP) induced by chemical or physical stress. The executioners of apoptosis are caspases, which cleave hundreds of cellular proteins, eventually leading to cell dismantlement [1]. In the process of apoptosis, the activation of executioner caspases was once considered as “a point of no return” [2]. However, in recent years, accumulating evidence demonstrates that cells can survive executioner caspase activation in response to apoptotic stress through a process named anastasis [3, 4]. Anastasis has been documented in multiple types of primary mouse cells and human cancer cell lines transiently exposed to apoptotic stimuli including ethanol, staurosporine, chemotherapeutic drugs and death receptor ligands [5–10]. One important question to ask is whether cells that survive executioner caspase activation differ from those that do not activate executioner caspases in response to apoptotic stimuli. Several reports suggest that anastasis may drive tumor initiation. Executioner caspases are essential for radiation- or Myc-induced genomic instability and carcinogenesis in human mammary epithelial cells [11, 12]. Anastatic NIH3T3 cells exhibit chromosome aberration and undergo oncogenic transformation after ethanol treatment [6]. Anastasis also causes change in cancer cells, but the features

cancer cells acquire after anastasis vary among different cancer types. Anastatic breast cancer cells and cervical cancer cells surviving exposure to chemotherapeutic drugs show increased drug resistance and migration [7]. Melanoma cells that survive executioner caspase activation induced by transient tBid over-expression or exposure to chemotherapeutic drug dacarbazine display elevated in vitro cell migration and in vivo metastasis but no difference in drug resistance [9].

Apoptosis induction is a common strategy to treat cancer. Many chemotherapeutic drugs kill cancer cells through inducing apoptosis, but tumor relapse and metastasis often occur after therapy [13]. In contrary to its tumor suppressive role, apoptosis is prevalent in gastric cancer, breast cancer, ovarian cancer, and lymphoma, and is often positively correlated with aggressiveness [1, 14–20]. Understanding how cancer cells survive apoptotic stress during cancer progression and chemotherapy can provide new targets for cancer therapy. In this study, we aim to investigate whether ovarian cancer cells can survive through anastasis in response to apoptotic stress and whether anastasis in ovarian cancer cells causes any phenotypic changes that may contribute to ovarian cancer progression. We employed two ovarian cancer cell lines, HEY and A2780 cells, and two apoptotic stimuli, a death receptor ligand TRAIL and a chemotherapeutic drug Paclitaxel which induces MOMP, to demonstrate that ovarian cancer cells can survive different types of apoptotic initiation through anastasis. Using a reporter system, mCasExpress, to label and

¹Key Laboratory of Experimental Teratology, Ministry of Education, Department of Histoembryology, School of Basic Medical Sciences, Cheeloo College of Medicine, Shandong University, Jinan 250012 Shandong, China. ²Key Laboratory of Experimental Teratology, Ministry of Education, Institute of Molecular Medicine and Genetics, School of Basic Medical Sciences, Cheeloo College of Medicine, Shandong University, Jinan 250012 Shandong, China. ³Molecular, Cellular and Developmental Biology Department, University of California, Santa Barbara, CA 93106, USA. ⁴State Key Laboratory of Radiation Medicine and Protection, Institute for Translational Medicine, Soochow University Suzhou Medical College, Suzhou 215123 Jiangsu, China. ✉email: sgp@sdu.edu.cn
Edited by M Piacentini

Received: 8 April 2022 Revised: 19 October 2022 Accepted: 20 October 2022
Published online: 29 November 2022

isolate anastatic cells, we show that the anastatic ovarian cancer cells acquire an increased degree of malignancy, manifested in the forms of enhanced tumor angiogenesis and metastasis. Mechanistically, these anastasis-induced phenotypic changes depend on p38, which is activated in response to apoptotic stress to promote survival and persists in the anastatic cells to confer increased aggressiveness.

MATERIALS AND METHODS

Cell culture and treatment

HEY cells (PROCELL, Cat# CL0671) and A2780 cells (Icell Company, Cat# h004) were cultured at 37°C, 5% CO₂ with DMEM (high glucose) (ThermoFisher Scientific, Cat# 11995-040) complemented with 10% fetal bovine serum (AusgeneX, Cat# FBS500-S), 100 U/mL penicillin and 100 µg/mL streptomycin (Spark Jade, Cat# CM0004-100ml). HUVECs (ICell, Cat# h110) were cultured at 37°C, 5% CO₂ with endothelial cell basal medium (Zhongqiaoxin Zhou Biotech, Cat# 1001) supplemented with 5% fetal bovine serum (Zhongqiaoxin Zhou Biotech, Cat# 0025), 1% Endothelial Cell Growth Supplement (ZhongqiaoXin Zhou Biotech, Cat# 1052), 100 U/mL penicillin and 100 µg/mL streptomycin (Zhongqiaoxin Zhou Biotech, Cat# 0503). All cells were routinely tested for mycoplasma. When treated, cells were randomly allocated into different treatment groups. Both adding chemicals to cell culture and removing chemicals were accompanied with medium replacement. In experiments with HEY-CasExpress or A2780-CasExpress cells, doxycycline (DOX) was applied to cell culture 6 h before addition of TRAIL, PTX or vehicle and removed together with them. In the experiments where kinase or caspase inhibitors were kept during TRAIL or PTX treatment and the following recovery phase, upon removal of TRAIL or PTX, the inhibitors were added again to recovery medium to ensure efficient inhibition during recovery. All the apoptosis inducers, kinase inhibitors and activators used in this work are listed in Supplementary Table S1.

Animals

4-week-old female nude (BALB/cNj-Foxn1^{nu}/Gpt, Strain# D000521) mice and NCG (NOD/ShiLtJGpt-Prkdc^{em26Cd52}Il2rg^{em26Cd22}/Gpt, Strain# T001475) mice were purchased from GemPharmatech (Jiangsu, China) and acclimated for 7 days in a specific-pathogen-free facility at 22°C and 40–50% humidity, with a 12/12 h light–dark cycle before experiments. Animals were randomly allocated into different groups. All animal experiments were conformed to the ethical guidelines and protocols approved by the Animal Care and Use Committee of Shandong University.

Conditioned medium collection

Cells were starved in 2% serum medium for 24 h. Conditioned medium was collected, centrifuged at 1000 g for 5 min and concentrated with 3kD ultrafiltration tubes (Millipore, UFC900396). Before applied to cell culture, the concentrated conditioned medium was filtered through 0.22 µm filters.

Plasmid construction

To construct pCW57-Lyn11-NES-DEVD-FlpO-hygro plasmid, FlpO was cloned from pCAG-FlpO plasmid (Addgene# 89574). Lyn11-NES-DEVD sequence (ggatgtataaaagctcaaaagggaaagacagcgGGTGGAAGTGGTctgccaccctctgagcgcctgaccctgGGTGGAAGTGGTtagaaaagcgatgagtgaggatggatgagtgatgagtgccgGGTGGAAGTGG) was synthesized by Integrated DNA Technologies (Iowa, USA). The two fragments were inserted into pCW57-MCS1-P2A-MCS2-hygro (Addgene# 80922) between NheI and BamHI using In-Fusion Cloning Kit (TakaraBio, Cat# 639650). To construct pCDH-FRT-STOP-FRT-ZsGreen plasmid, FRT-STOP-FRT fragment was PCR amplified using pJFRC206-10XUAS-FRT-STOP-FRT-myr:smGFP:V5 (Addgene# 63168) as template. ZsGreen fragment was cloned from pLVX-shRNA2-ZsGreen vector (Clontech, Cat# 632179). The pCDH-puro vector was obtained by removing the GC3AI sequence from pCDH-puro-CMV-GC3AI (Addgene# 78910). The FRT-STOP-FRT fragment and the ZsGreen fragment were then ligated into pCDH-puro vector using In-Fusion Cloning Kit (TakaraBio, Cat# 639650).

Virus production and infection

HEK293T cells were transfected with pCDH-puro-CMV-GC3AI (Addgene# 78910), pCDH-FRT-STOP-FRT-ZsGreen-puro or pCW57-Lyn11-NES-DEVD-flpO-hygro with pCMV-dR8.2 dvpr (Addgene# 8455) and pCMV-VSV-G

(Addgene# 8454) using Lipofectamine 3000 (Invitrogen, Cat# 13778150). The supernatant was harvested and filtered with a 0.45 µm filter at 48 h and 72 h post transfection. Ovarian cancer cells were infected overnight in the presence of 10 µg/mL polybrene and then selected for 5–7 days in growth medium containing 2 µg/mL puromycin and/or 250 µg/mL hygromycin.

siRNA transfection

Double-stranded RNA against *MAPK14* was purchased from GenePharma. The sequence was listed in Supplementary Table S2. Transfection of cells was conducted with Lipofectamine RNAiMAX Reagent (Thermo Fisher Scientific, Cat# 13778030). Cells or conditioned medium were collected at 24 h or 48 h after siRNA delivery for the following transwell assays or HUVEC tube formation experiments.

Flow cytometry and cell sorting

HEY or A2780 cells carrying GC3AI or mCasExpress were harvested after treatment and recovery and stained with 1 µg/ml 7-AAD (ThermoFisher Scientific, Cat# A1310). Flow cytometry was done on Beckman CytoFLEX (Beckman Coulter, Indianapolis, IN, US) and cell sorting was done on Beckman MoFlo (Beckman Coulter, Indianapolis, IN, US).

RNA sequencing

Total RNA was extracted using Trizol (ThermoFisher Scientific, Cat# 15596-026) according to the manufacturer's protocol. RNA quality was evaluated on an Agilent 2100 Bioanalyzer (Agilent Technologies, Palo Alto, CA, US) and checked using RNase free agarose gel electrophoresis. mRNA was enriched using Oligo(dT) beads, fragmented using fragmentation buffer and reversely transcribed into cDNA using NEBNext Ultra RNA Library Prep Kit for Illumina (New England Biolabs, Cat# 7530). The purified double-stranded cDNA fragments were end repaired, A base added, and ligated to Illumina sequencing adapters. The ligation products were purified using the AMPure XP Beads (1.0×). Ligated fragments were subjected to size selection by agarose gel electrophoresis and PCR amplification. The cDNA library was sequenced using Illumina Novaseq6000 by Gene Denovo Biotechnology Co. (Guangzhou, China).

RNA extraction and qRT-PCR

5 × 10⁵ Cells were seeded in one well of a 6-well plate at 24 h before experiments. RNA was extracted using RNA Rapid Extraction Kit (Spark Jade, Cat# Ac1001). Quantitative real-time polymerase chain reaction (qRT-PCR) was performed using the Real-time PCR system (Vanzyne, Cat# Q411-03) and Analytikjena qTOWER. The primers used are listed in the Supplementary Table S3.

Western Blot

1.0 × 10⁶ cells were seeded at 24 h before experiments. Cell lysates were prepared with RIPA buffer (Beyotime, Cat# P0013B) supplemented with 1 mM PMSF. Protein concentrations were measured with the BCA assay kit (Spark Jade, Cat# EC0001). 30 µg proteins were applied to SDS-PAGE then transferred to PVDF membranes. The membranes were incubated with primary antibody (1:1000) overnight at 4°C and then with the secondary antibody (1:2000) at room temperature for 1 h. Proteins were detected using Chemiluminescent Substrates (Spark Jade, Cat# ED0016) and Tanon 5200 Multi Chemiluminescence imager (Tanon Science & Technology Co., Shanghai, China). The antibodies used are listed in the Supplementary Table S4. All the uncropped blots are shown in "Original Western Blots" file.

Transwell assay

The transwell assays were performed using 8 µm transwell chambers (Falcon, Cat# 353097). About 2.5 × 10⁴ HEY or HUVECs or 5 × 10⁴ A2780 cells were seeded into the upper chamber in 100 µL serum-reduced Opti-MEM (ThermoFisher Scientific, Cat# 31985-088). The lower chamber was filled with 500 µL medium containing 10% FBS (for HEY and A2780 cells) or 300 µL conditioned medium (10× concentrated) plus 200 µL serum-reduced Opti-MEM (for HUVECs). After 24 h (for HEY cells and HUVECs) or 48 h (for A2780 cells) incubation, the cells were fixed with 4% paraformaldehyde at room temperature for 10 min. After staining with crystal violet (Solarbio, Cat# G1065), cells that migrated were imaged using IX73 (Olympus, Japan).

HUVEC tube formation assay

Matrigel (BD Biosciences, Cat# 354234) was defrosted and aliquoted into 96-well plates at 50 μ L/well with pre-chilled tips. The plates were then placed in a 37 °C incubator for 1 h to allow Matrigel to solidify. HUVECs were suspended in medium containing conditioned medium (10 \times concentrated) and seeded into the Matrigel-coated plates at 3×10^4 cells/well. The 96-well plates were centrifuged to make HUVECs settle down to the bottom of the wells. After 2–4 h, the cells were imaged using IX73 (Olympus, Japan), and the tube length was analyzed using Image J software.

EdU incorporation assay

Cells were seeded in 6-well plates with coverslips. After treatment, cells were washed once with PBS. EdU incorporation and staining were performed using BeyoClick EdU-594 kit (Beyotime, Cat# C00785) according to the manufacturer's protocol. The images were acquired on BX51 (Olympus, Japan).

CCK-8 assay

Cell proliferation rates were measured by the Cell Counting Kit-8 (CCK-8) assay (Spark Jade, Cat# CT0001). Approximately 4×10^4 cells were seeded in 96-well plates with 100 μ L medium per well. After 24 h, 48 h, and 72 h, 10 μ L CCK-8 solution was added to each well and incubated for 2–4 h in dark. The absorbance at 450 nm was measured by Molecular Devices Reader (Emax Plus, US).

ELISA

Ovarian cancer cells were seeded in 6-well plates at 90% confluency. 24 h later, the medium was collected and centrifuged at 1000 g for 5 min. The concentrations of PGE2 (Meimian, Cat# MM0162H2), TNF- α (Meimian, Cat# MM0122H2), VEGFA (Meimian, Cat# MM-14698H2) and VEGFC (Meimian, Cat# MM-0113H2) in the medium were detected by ELISA kits.

In vivo Matrigel implant assay

Matrigel (BD Biosciences, Cat# 354234) mixed with conditioned medium (100 \times concentrated) collected from different cell populations were injected subcutaneously into 5-week-old female nude mice. After one week, the mice were sacrificed and the Matrigel implants were excised to assess the angiogenesis. The formation of neovessels was determined by measuring the hemoglobin content using Drabkin's reagent kit (Sigma, Cat# 5941) according to the manufacturer's protocol. Four mice were used for each group. The experiments were repeated twice independently.

Subcutaneous xenograft tumor model

1×10^6 HEY cells or 5×10^6 A2780 cells were suspended with 100 μ L PBS and injected subcutaneously into female NCG mice. Tumor dimensions were measured every other day and the tumor volume was determined using the formula $1/2 \times \text{length} \times \text{width}^2$. When the largest tumor reached the maximum allowed size, mice were sacrificed. The tumors were weighted, photographed and fixed in 4% paraformaldehyde for histological analysis.

Peritoneal metastasis model

5×10^6 HEY cells or 1×10^7 A2780 cells carrying luciferase were suspended in 100 μ L PBS and injected into abdominal cavity of female NCG mice. After 2 or 4 weeks, the mice were imaged using IVIS Spectrum In Vivo Imaging System (PerkinElmer, US). After the tumor growth was confirmed, the mice were sacrificed. The tumor nodules in the peritoneal cavity and the internal organs including livers, diaphragms, kidneys, stomach and intestines were collected, weighed, fixed and subjected to Hematoxylin-Eosin staining.

Immunohistochemistry

The tumors were bisected. The midline sections were immunostained for CD31 and Ki67. The tissue sections were subjected to antigen retrieval with citric acid (PH6.0) antigen retrieval buffer and washed with PBS three times. Activity of endogenous peroxidase was blocked by 3% hydrogen peroxide incubation for 10 min. 3% BSA was used in blocking for 30 min at room temperature. Primary antibodies were incubated overnight at 4 °C. Secondary antibodies were incubated at room temperature for 50 min. The staining was visualized using diaminobenzidine and counterstained with hematoxylin. The stained sections were

imaged on BX51 (Olympus, Japan). The antibodies used are listed in Supplementary Table S4.

Statistical analysis and reproducibility

Data are presented as the mean \pm standard error of the mean (SEM). Statistical significance was determined using one-way ANOVA. The Tukey test was used to derive adjusted *P*-value for multiple comparisons. *P* < 0.05 was considered as statistically significant. The assumption of equal variance was validated by F-test. Statistical analyses were performed using GraphPad Prism version 8 (GraphPad Software). The sample sizes were chosen empirically based on the observed effects and previous reports. The sample size for each experiment is listed in the figure legends. When collecting and analyzing data of RT-qPCR, immunostaining and xenograft volumes, the investigators were blinded to the group allocation. All the experiments except those involving mice were repeated at least three times. The experiments involving mice were repeated twice. All the repeats were successful, and the representatives were shown in the figures.

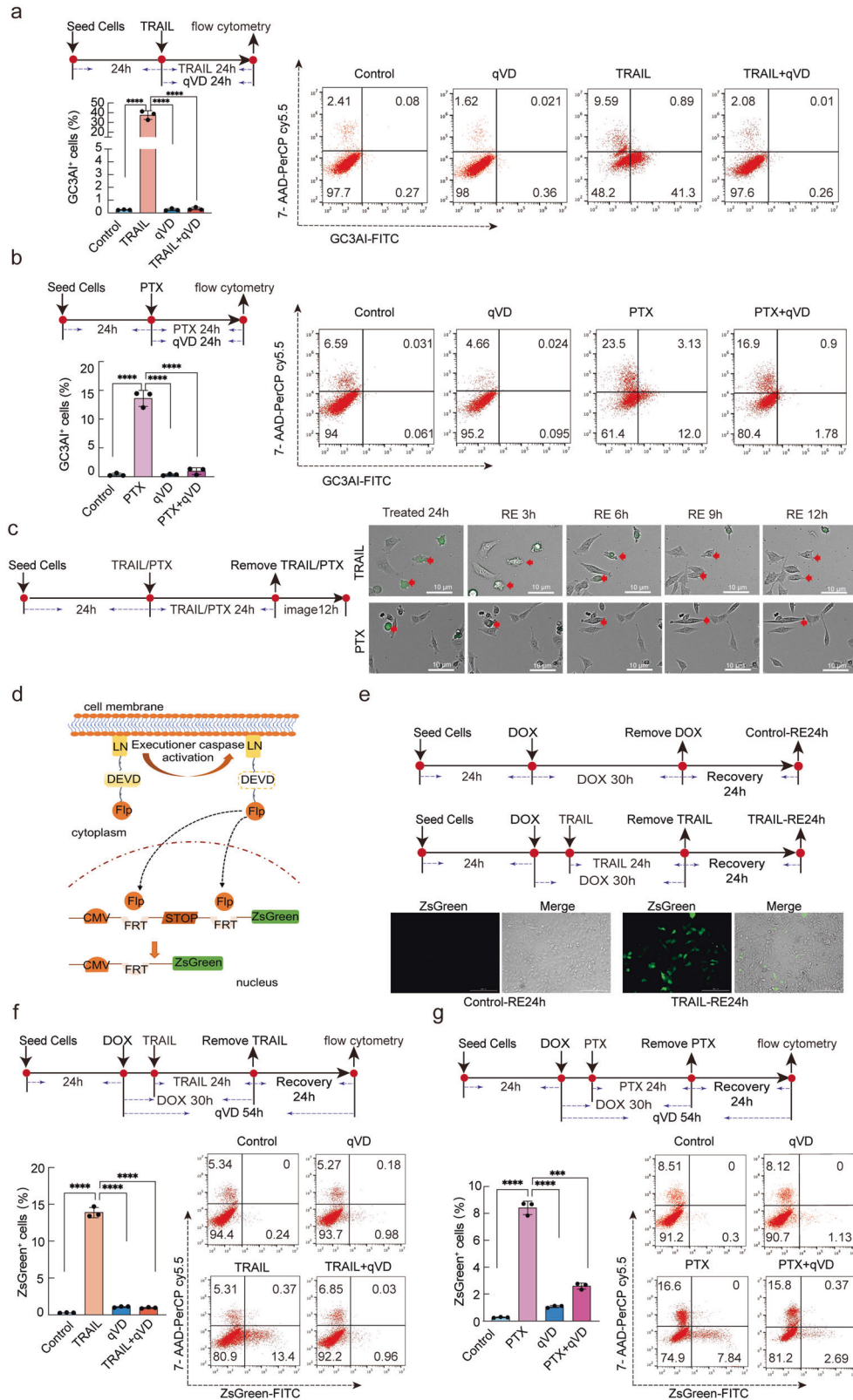
RESULTS

Ovarian cancer cells undergo anastasis after TRAIL or Paclitaxel treatment

To investigate whether ovarian cancer cells can survive apoptotic executioner caspase activation, we generated HEY cells stably expressing a live reporter for executioner caspase activity, GC3AI [21] (designated HEY-GC3AI cells). The GC3AI reporter emits fluorescence upon executioner caspase activation [21]. Treatment of TRAIL or Paclitaxel (PTX) for 24 h resulted in executioner caspase activation (GC3AI⁺) in 38% and 14% of HEY-GC3AI cells, respectively, which was abolished by co-treatment with pan-caspase inhibitor Q-VD-OPh (qVD) (Fig. 1a, b). Through live imaging, we found both TRAIL and PTX treatment induced morphological changes characteristic of apoptosis as well as activation of executioner caspases indicated by the green fluorescence (Fig. 1c). After 24 h treatment, we replaced the stimulus-containing medium with fresh culture medium to allow the cells to recover. While many cells died, some green shrunk cells gradually spread out (Fig. 1c, the red arrows), indicative of ongoing anastasis. Anastasis was also observed in another ovarian cancer cell line A2780 after 24 h exposure to TRAIL (Supplementary Fig. S1a, c) or PTX (Supplementary Fig. S1b, c), suggesting anastasis is a general response to executioner caspase activation in ovarian cancer cells.

mCasExpress reporter labels cells that have experienced executioner caspase activation and their descendants

The GC3AI reporter can monitor the live executioner caspase activity, but the labeled cells gradually lose the green fluorescence after recovery due to the diminished caspase activity (Fig. 1c, Supplementary Fig. S1c), making the reporter unsuitable for long-term tracing. Therefore, we modified the previously published *Drosophila* lineage tracing system for executioner caspase activation, CasExpress [22], for its utility in mammalian cells. The mammalian CasExpress (mCasExpress) is comprised of two elements, the executioner caspase-activated DNA recombinase Flp (Lyn11-NES-DEVD-Flp) and a Flp activity reporter (FRT-STOP-FRT-ZsGreen). In cells without executioner caspase activity, the caspase-activated Flp is kept in cytosol by the Lyn11 and nuclear export signal (NES) sequences. In cells with executioner caspase activation, the DEVD site between Flp and Lyn11-NES (LN) sequences will be cleaved, resulting in nuclear translocation of Flp, which in turn leads to removal of the transcriptional termination signal between the two FRT sites and the subsequent expression of green fluorescent protein ZsGreen (Fig. 1d). Thus, using mCasExpress biosensor, cells that have experienced executioner caspase activation as well as their daughter cells will be labeled with green fluorescence (designated ZsGreen⁺ cells). Some cultured cells may have basal level of caspase activity or



experience transient caspase activation during *in vitro* culture. To minimize the accumulation of ZsGreen⁺ cells during culture, we placed the caspase-activated Fip under the control of a doxycycline (DOX)-inducible promoter. ZsGreen⁺ cells were observed in HEY cells carrying mCasExpress (HEY-CasExpress)

recovered from TRAIL treatment but not in those recovered from mock treatment (Fig. 1e). At the end of 24 h recovery, about 14% of the attached cells in the TRAIL-treated group were ZsGreen⁺ while in mock-treated group only 0.2% were ZsGreen⁺ (Fig. 1f). Inhibition of caspase activity by qVD during TRAIL treatment and

Fig. 1 HEY cells undergo anastasis after TRAIL or Paclitaxel (PTX) treatment. **a** The representative images and quantifications of flow cytometry data showing the percentage of GC3AI⁺ cells in HEY-GC3AI cells after 24 h treatment of control (0.1% DMSO), 50 μ M qVD, 400 ng/ μ l TRAIL, or 400 ng/ μ l TRAIL + 50 μ M qVD. **b** The representative images and quantifications of flow cytometry data showing the percentage of GC3AI⁺ cells in HEY-GC3AI cells after 24 h treatment of control (0.1% DMSO), 50 μ M qVD, 1 μ M PTX, or 1 μ M PTX + 50 μ M qVD. **c** Time-lapse live imaging of HEY-GC3AI cells after 24 h treatment (Treated 24 h) of TRAIL or PTX, and after recovery for 3 h (RE 3 h), 6 h (RE 6 h), 9 h (RE 9 h) and 12 h (RE 12 h). The red arrows point to the cells recovering from executioner caspase activation. The green indicates executioner caspase activity. **d** The schematic of mCasExpress. LN: Lyn11-NES. **e** Images of HEY-CasExpress cells after 24 h recovery from TRAIL or control treatment showing ZsGreen signals in recovered cells. HEY-CasExpress cells were treated with TRAIL for 24 h and replaced with fresh culture medium to allow the cells to recover for another 24 h. 1 μ g/ml DOX was applied to the cells 6 h before TRAIL treatment, kept in the treatment medium and removed together with TRAIL. The control cells were incubated with 1 μ g/ml DOX for 30 h and then grown in fresh culture medium without DOX for 24 h. **f** The representative images and quantifications of flow cytometry data showing the percentage of ZsGreen⁺ cells in HEY-CasExpress cells after 24 h treatment of control (0.1% DMSO), 50 μ M qVD, 400 ng/ μ l TRAIL, or 400 ng/ μ l TRAIL + 50 μ M qVD plus 24 h recovery. **g** The representative images and quantifications of flow cytometry data show the percentage of ZsGreen⁺ cells in HEY-CasExpress cells after 24 h treatment of control (0.1% DMSO), 50 μ M qVD, 1 μ M PTX, or 1 μ M PTX + 50 μ M qVD plus 24 h recovery. In **f** and **g**, qVD was added together with DOX and kept in the culture till the end of 24 h recovery. $n = 3$ in all the bar graphs. Data are presented as the mean \pm SEM. *** $P < 0.001$. **** $P < 0.0001$.

recovery strongly reduced TRAIL-induced ZsGreen⁺ cells (Fig. 1f), indicating that the ZsGreen⁺ cells detected after recovery from TRAIL treatment were those that had undergone anastasis. The caspase-dependent ZsGreen⁺ living cells were also detected in HEY-CasExpress cells recovered from PTX treatment (Fig. 1g), A2780-CasExpress cells recovered from TRAIL (Supplementary Fig. S1d) or PTX treatment (Supplementary Fig. S1e), though the percentage of ZsGreen⁺ cells varied under different conditions.

Anastasis enriches transcriptome in migration and angiogenesis

To investigate whether anastasis grants ovarian cancer cells any new features, for each treatment-cell line combination, we sorted the ZsGreen⁺ cells, which survived treatment-induced executioner caspase activation (anastatic), and the ZsGreen⁻ counterpart population, which experienced the same treatment but did not activate executioner caspases, after 24 h recovery and cultured them separately. The cells treated with DOX and vehicle control were also subjected to sorting and collected as control populations (Fig. 2a). We designed primers flanking the *FRT-STOP-FRT-ZsGreen* cassette to confirm the purity of the isolated cell populations after long-term in vitro culture. The results showed that all ZsGreen⁺ cells had the STOP cassette removed whereas all ZsGreen⁻ and control populations kept the STOP cassette after in vitro culture for more than five passages (Supplementary Fig. S2a). These established cultures were used in the following transcriptome profiling and phenotypic analyses.

To identify the global expressional changes caused by anastasis, we performed RNA sequencing on the ZsGreen⁺ and ZsGreen⁻ populations established from HEY-CasExpress cells recovered after 24 h PTX treatment (designated as HEY-PTX-ZsGreen⁺ and HEY-PTX-ZsGreen⁻, respectively), and the control population from HEY-CasExpress cells recovered after 24 h treatment with vehicle control (0.1% DMSO) (designated as HEY-control^P). The PCA analysis revealed that these three populations had distinct transcriptomes (Fig. 2b). 252 genes were differentially expressed in HEY-PTX-ZsGreen⁺ cells and HEY-PTX-ZsGreen⁻ cells (Fig. 2c). Gene ontology (GO) analysis revealed that the differentially expressed genes (DEGs) between HEY-PTX-ZsGreen⁺ population and HEY-PTX-ZsGreen⁻ population, as well as those between HEY-PTX-ZsGreen⁺ population and HEY-control^P population, were enriched in GO terms related to cell migration and angiogenesis (Fig. 2d, Supplementary Fig. S2b, c). The KEGG pathway enrichment analysis showed that pathways “cytokine-cytokine receptor interaction”, “TNFR signaling pathway”, and “IL-17 signaling pathway” were enriched in HEY-PTX-ZsGreen⁺ cells when compared to HEY-PTX-ZsGreen⁻ and HEY-control^P cells (Fig. 2e, Supplementary Fig. S2d). We validated the expressional changes of 18 genes that belong to the GO term “cell migration” and “angiogenesis” by RT-qPCR. Expression of 14 genes was

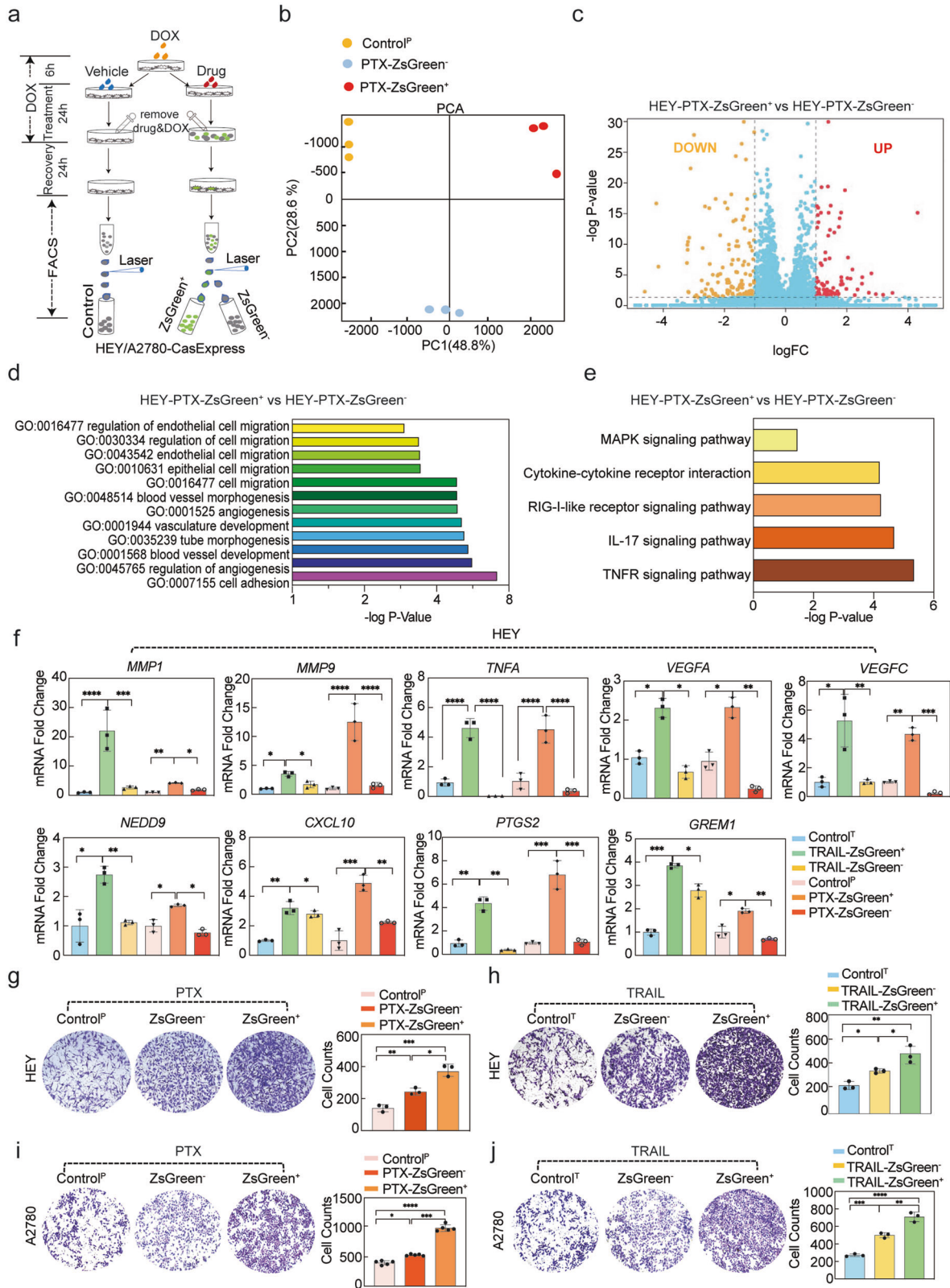
upregulated in HEY-PTX-ZsGreen⁺ cells compared to that in HEY-PTX-ZsGreen⁻ cells and HEY-control^P cells (Fig. 2f, Supplementary Fig. S2f). Among these 14 genes, 9 were also increased in the ZsGreen⁺ populations derived from other treatment-cell line combinations (Fig. 2f, Supplementary Fig. S2e), suggesting that genes related to migration and angiogenesis may be generally upregulated in anastatic ovarian cancer cells.

Anastatic ovarian cancer cells acquire enhanced migratory capacity

The upregulated expression of migration-related genes in HEY-PTX-ZsGreen⁺ cells prompted us to evaluate their migration capacity. Transwell assay showed that HEY-PTX-ZsGreen⁺ cells migrated faster than HEY-PTX-ZsGreen⁻ cells, and the latter were more migratory than HEY-control^P cells (Fig. 2g). Similar difference in migration was also observed in the control, ZsGreen⁺ and ZsGreen⁻ populations derived from other treatment-cell line combinations (Fig. 2h–j). These data suggest exposure to apoptotic stimuli induces elevated migration in ovarian cancer cells, which is further enhanced by executioner caspase activation.

Anastatic ovarian cancer cells secrete more pro-angiogenic factors

Consistent with the increased *VEGFA*, *VEGFC*, *PTGS2* and *TNFA* mRNA levels in the anastatic cells (Fig. 2f, Supplementary Fig. S2e), elevated levels of secreted VEGFA, VEGFC, TNF α and PGE2 were detected in the medium of the ZsGreen⁺ populations compared to those in the medium of the ZsGreen⁻ populations and the control populations (Fig. 3a, Supplementary Fig. S3a), indicating that the anastatic cells produce more pro-angiogenic factors. We then collected the conditioned medium from the ZsGreen⁺, the ZsGreen⁻ and the control cell culture, respectively, and evaluated their effects on proliferation, migration and in vitro tube formation of human umbilical vein endothelial cells (HUVECs). HUVECs incubated with the conditioned medium from different populations exhibited similar growth rate (Supplementary Fig. S4). HUVECs incubated with medium conditioned by the ZsGreen⁺ cells displayed increased migration and tube formation than those incubated with medium conditioned by the other two types of cells (Fig. 3b–e, Supplementary Fig. S3b–e). To evaluate whether the conditioned medium from the ZsGreen⁺ populations are more angiogenic in vivo, we performed Matrigel implant assay. The conditioned medium was subcutaneously co-injected with Matrigel to nude mice. After one week, the Matrigel plugs mixed with the medium conditioned by the ZsGreen⁺ cells were found to contain more blood vessels than those mixed with the medium conditioned by the ZsGreen⁻ or the control cells (Fig. 3f–i, Supplementary Fig. S3f–i). These data together indicate that the anastatic ovarian cancer cells possess increased capability to induce angiogenesis.



Tumors formed by anastatic ovarian cancer cells exhibit enhanced angiogenesis and growth in vivo

Next, we tested whether the anastatic cells promote tumor angiogenesis and growth in vivo. We subcutaneously injected cells from the ZsGreen⁺ populations, the counterpart ZsGreen⁻

populations and the control populations to the NCG mice. The tumors formed by the ZsGreen⁺ cells grew faster (Fig. 4a–c, h–j, Supplementary Fig. S5a–c, h–j) and contained more proliferative cells (Fig. 4d, e, k, l, Supplementary Fig. S5d, e, k, l) and blood vessels (Fig. 4f, g, m, n, Supplementary Fig. S5f, g, m, n) when

Fig. 2 Anastasis enriches transcriptome in migration and angiogenesis and renders ovarian cancer cells more migratory. **a** The schematic of sorting ZsGreen⁺, ZsGreen⁻ and control populations from HEY/A2780-CasExpress cells after treatment with TRAIL or PTX (Drug) or vehicle control (Vehicle) plus 24 h recovery. FACS: fluorescence activated cell sorting. **b** Principal component analysis (PCA) of the RNA sequencing data. Volcano plot (**c**), GO enrichment (**d**) and KEGG pathway enrichment (**e**) of the DEGs between HEY-PTX-ZsGreen⁺ cells and HEY-PTX-ZsGreen⁻ cells. **f** mRNA expression of 9 migration- or angiogenesis-related genes in the indicated groups. $n = 3$. **g–j** Results of transwell assays of the indicated populations. In each panel, on the left are the representative images and on the right are the quantifications. $n = 3$ in **g**, **h**, and **j**. $n = 5$ in **i**. Data are presented as the mean \pm SEM. * $P < 0.05$; ** $P < 0.01$; *** $P < 0.001$; **** $P < 0.0001$. The control^T population is derived from the ZsGreen⁻ cells isolated from cells recovered from mock treatment (growth medium only) for TRAIL. The control^P population is derived from the ZsGreen⁻ cells isolated from cells recovered from mock treatment (0.1% DMSO) for PTX.

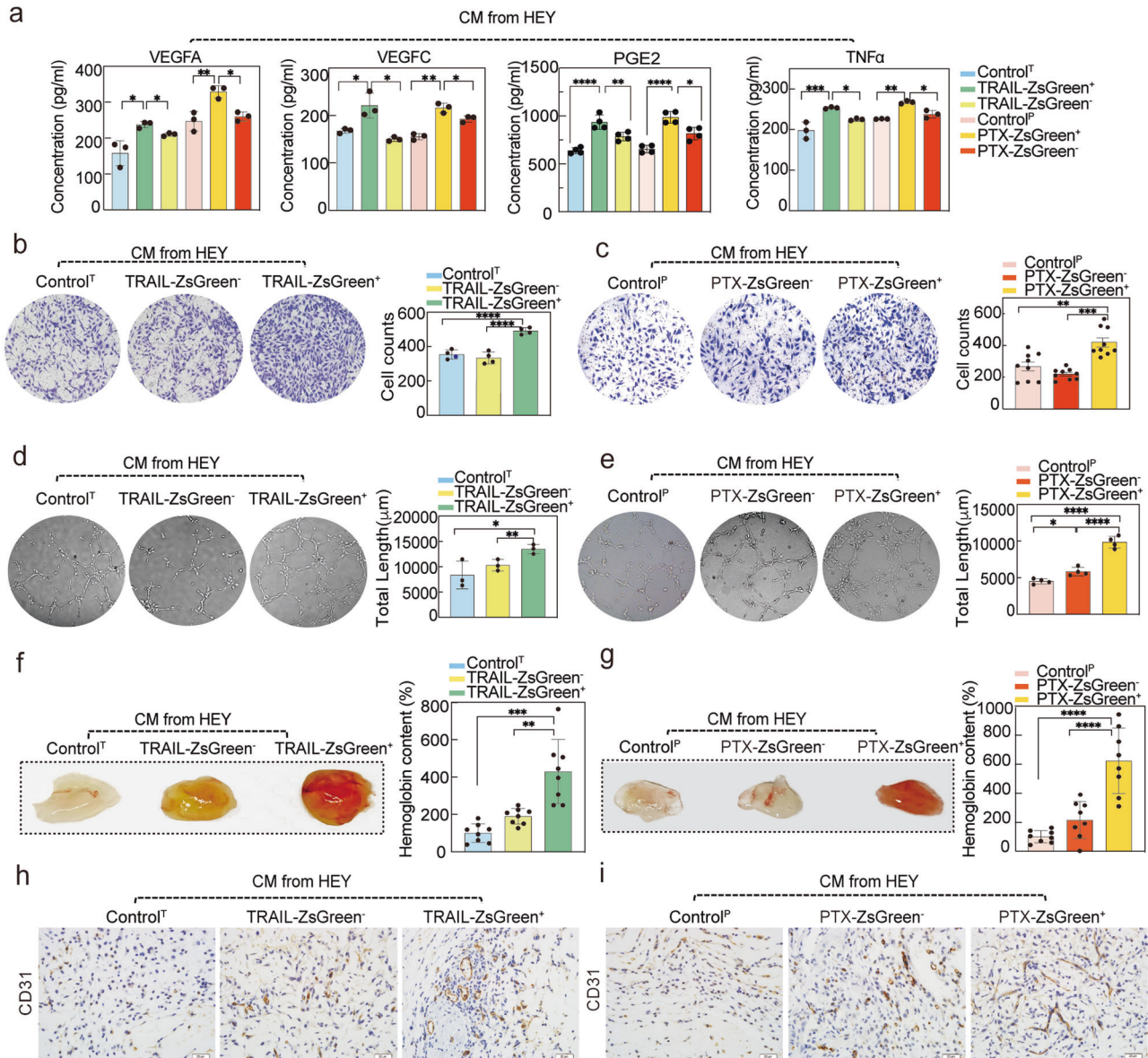


Fig. 3 Anastatic HEY cells secrete more pro-angiogenic factors. **a** The concentration of VEGFA ($n = 3$), VEGFC ($n = 3$), PGE2 ($n = 4$) and TNF α ($n = 3$) in the conditioned medium (CM) from the indicated populations. **b, c** The results of transwell assays to show migration of HUVECs induced by CM collected from the indicated populations. On the left are the representative images and on the right are the quantifications. $n = 4$ in **b**. $n = 9$ in **c**. **d, e** The results of tube formation of HUVECs induced by CM collected from the indicated populations. On the left are the representative images and on the right are the quantifications. $n = 3$ in **d** and $n = 4$ in **e**. **f, g** The results of Matrigel implant assays to show the in vivo angiogenesis triggered by CM from the indicated populations. On the left are the representative images of the Matrigel implants and on the right are the quantifications of Hemoglobin content in the Matrigel implants. $n = 8$. **h, i** The representative images of CD31 staining in the sections of the Matrigel implants. The scale bar is 20 μ m. Data are presented as the mean \pm SEM. * $P < 0.05$; ** $P < 0.01$; *** $P < 0.001$; **** $p < 0.0001$.

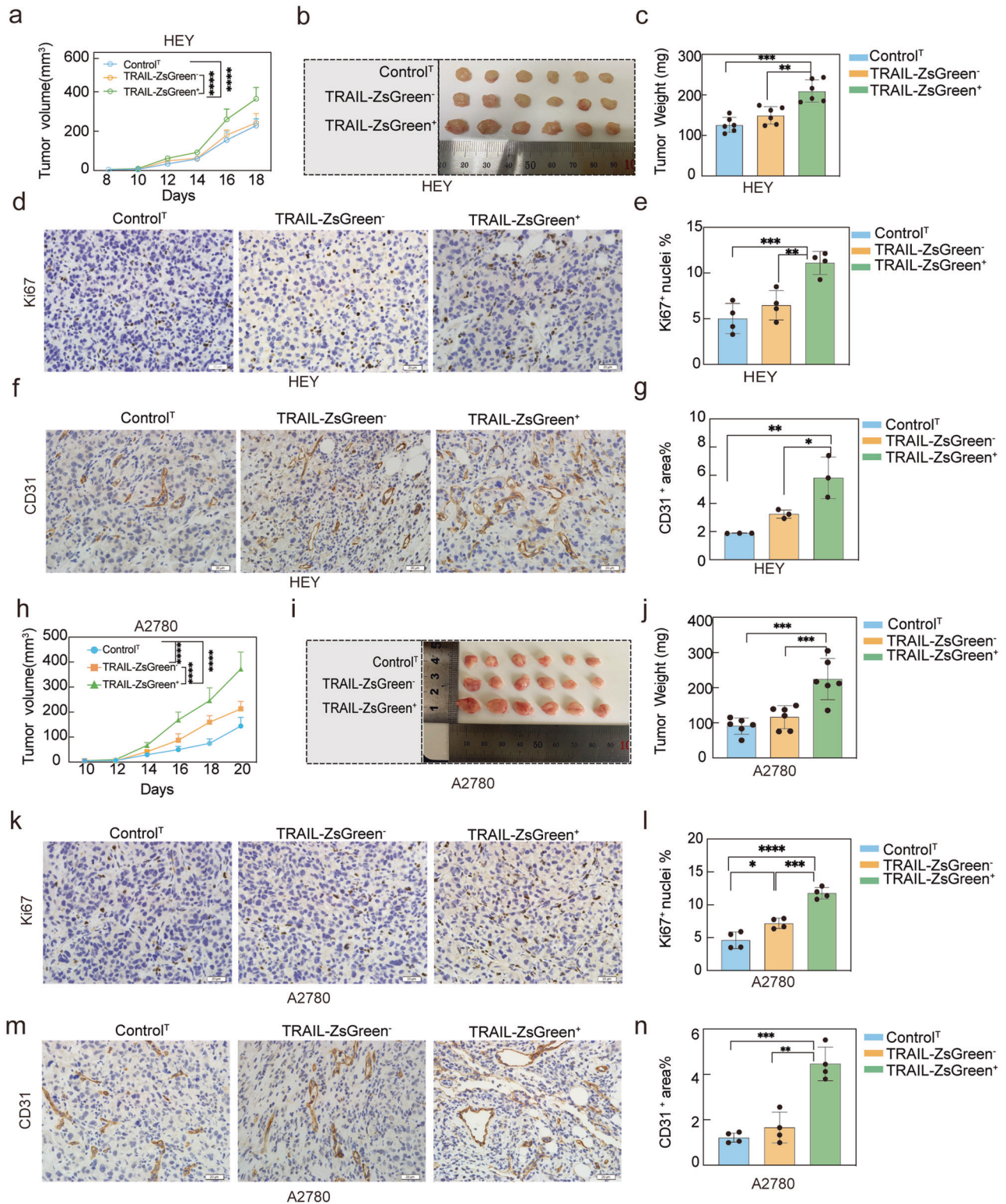


Fig. 4 Tumors formed by anastatic ovarian cancer cells exhibit enhanced growth and angiogenesis. **a** Change of the volume of the xenografts formed by HEY-control^T, HEY-TRAIL-ZsGreen⁻ or HEY-TRAIL-ZsGreen⁺ populations over time. $n = 6$. **b** Image of the collected xenografts. **c** The weight of the xenografts in **b**. $n = 6$. **d** The representative images of Ki67 staining in xenografts. **e** Quantification of the percentage of Ki67⁺ cells. $n = 4$. **f** The representative images of CD31 staining in xenografts. **g** Quantification of the percentage of CD31⁺ area. $n = 3$. **h** Change of the volume of the xenografts formed by A2780-control^T, A2780-TRAIL-ZsGreen⁻ or A2780-TRAIL-ZsGreen⁺ populations over time. **i** Image of the collected xenografts. **j** The weight of the xenografts in **i**. $n = 6$. **k** The representative images of Ki67 staining in xenografts. **l** Quantification of the percentage of Ki67⁺ cells. $n = 4$. **m** The representative images of CD31 staining in xenografts. **n** Quantification of the percentage of CD31⁺ area. $n = 4$. The scale bars in **d**, **f**, **k**, and **m** are 20 μm . Data are presented as the mean \pm SEM. * $P < 0.05$; ** $P < 0.01$; *** $P < 0.001$; **** $P < 0.0001$.

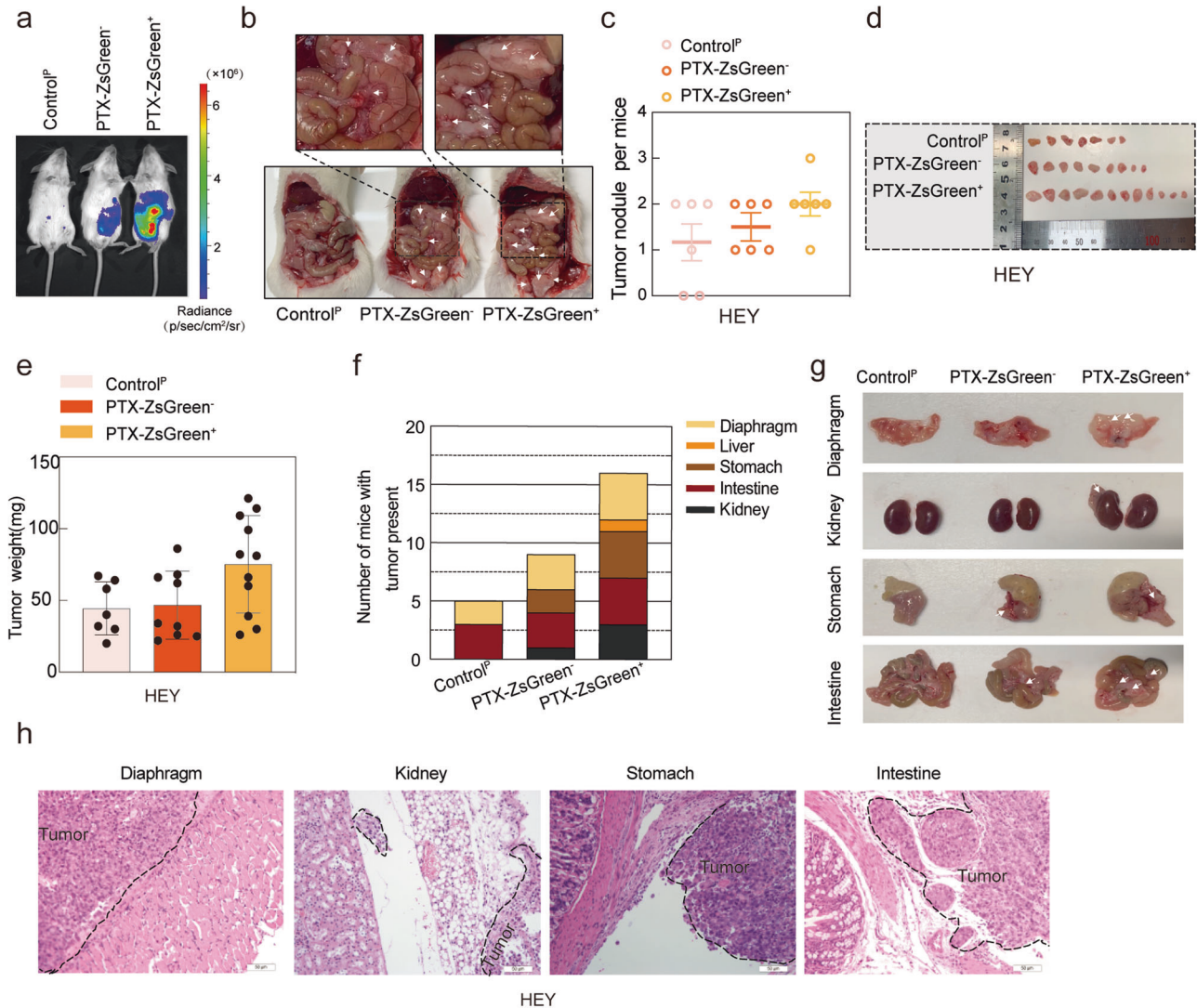


Fig. 5 Anastatic HEY cells exhibit elevated in vivo metastasis. **a** The representative luciferase images of live mice injected with HEY-control^P, HEY-PTX-ZsGreen⁻ or HEY-PTX-ZsGreen⁺ populations, respectively, to show the intraperitoneal growth and dissemination of tumors in vivo. **b** The representative images to show the tumors formed on the internal organs. The white arrows point to tumors. **c** Quantification of the number of the tumor nodules in the peritoneal cavity but not attaching to any internal organs in each mouse. *n* = 6. **d** The image of the tumor nodules in the peritoneal cavity but not attaching to any internal organs. **e** The weight of the tumor nodules collected from the peritoneal cavity of mice in the control^P (*n* = 7), PTX-ZsGreen⁻ (*n* = 9) and PTX-ZsGreen⁺ (*n* = 11) groups. **f** The number of mice with tumors metastasize to the indicated organs. **g** The representative images of the indicated organs from mice in all three groups. The white arrows point to the tumors. **h** Hematoxylin & Eosin (H&E) staining of different organs from mice injected with HEY-PTX-ZsGreen⁺ cells. The tumor areas are outlined with dashed black lines. In **c** and **e**, data are presented as the mean ± SEM.

compared to the tumors formed by the other two types of cells. These data indicate that anastatic cells promote tumor growth and angiogenesis better than cells with no experience of executioner caspase activation. Given that the in vitro growth rates of the ZsGreen⁺, the ZsGreen⁻ cells and the control cells were similar (Supplementary Fig. S6), the enhanced growth of tumors formed by the anastatic cells may be attributed to their pro-angiogenic capacity.

Anastatic cells are more metastatic in vivo

The enhanced migration and angiogenic capacity of the anastatic cells suggest that they may exhibit increased metastasis in vivo. To verify this speculation, we introduced luciferase to HEY-PTX-ZsGreen⁺, HEY-PTX-ZsGreen⁻ and HEY-control^P cells using lentivirus and intraperitoneally injected them into the NCG mice. We then monitored the tumor growth and dissemination in vivo, and found that two weeks after injection,

the number and the weight of the peritoneal disseminated nodules formed by HEY-PTX-ZsGreen⁺ cells were higher than those formed by the other two groups (Fig. 5a–e). HEY-PTX-ZsGreen⁺ cells also exhibited more metastasis to diaphragm, stomach, liver, kidney and intestine (Fig. 5f–h). Similar enhancement of in vivo metastasis in the ZsGreen⁺ population was also observed in HEY cells recovered from TRAIL treatment (Supplementary Fig. S7). These data indicate that ovarian cancer cells derived from anastasis acquire increased metastatic capability in vivo.

The elevated production of pro-angiogenic factors in anastatic cells relies on increased p38 activity

The next question to ask is what accounts for the increased angiogenic capacity in the anastatic cells. It has been reported that activated caspase-3 can trigger expression of pro-angiogenic genes [23, 24]. However, none of the ZsGreen⁺, the ZsGreen⁻ and

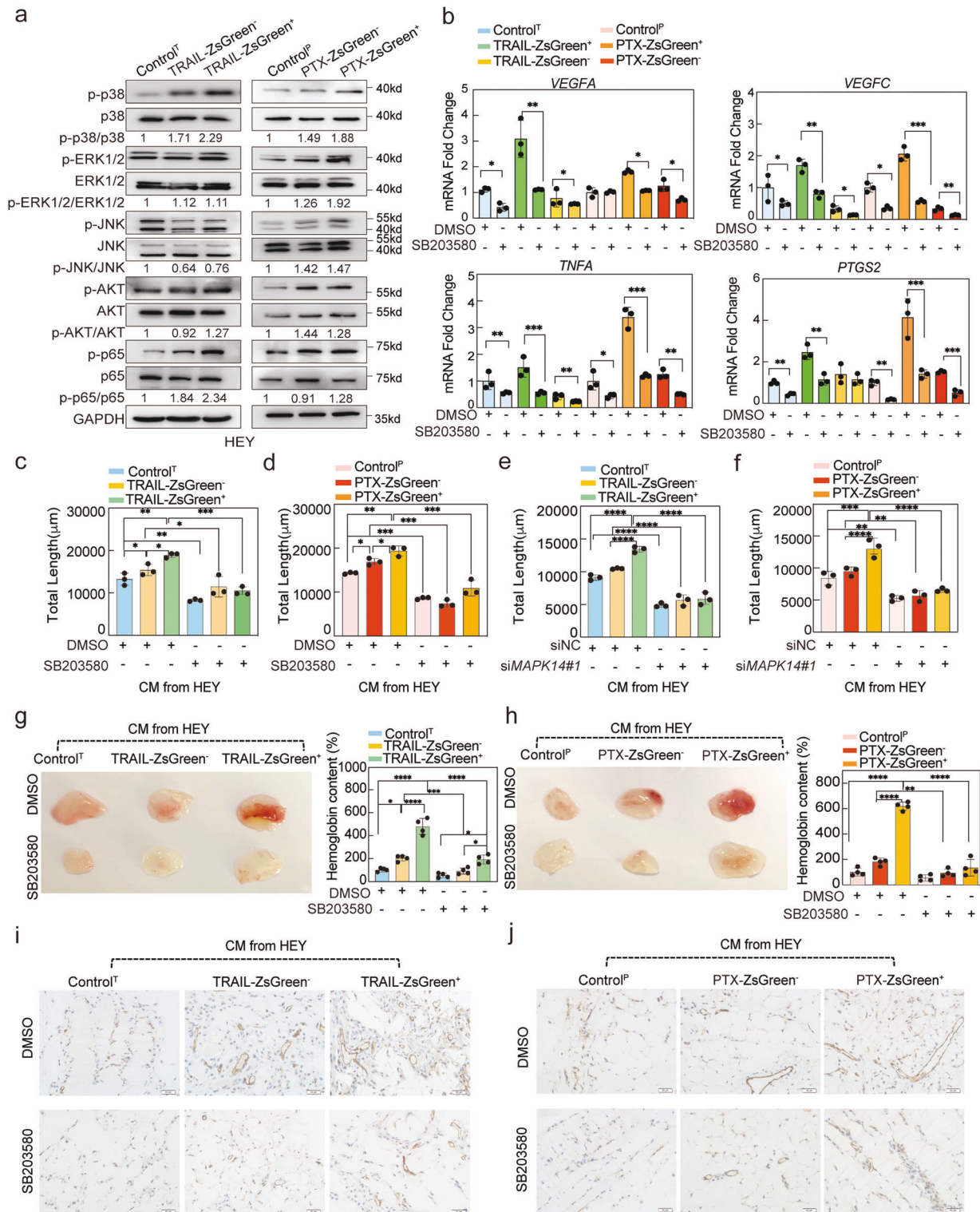
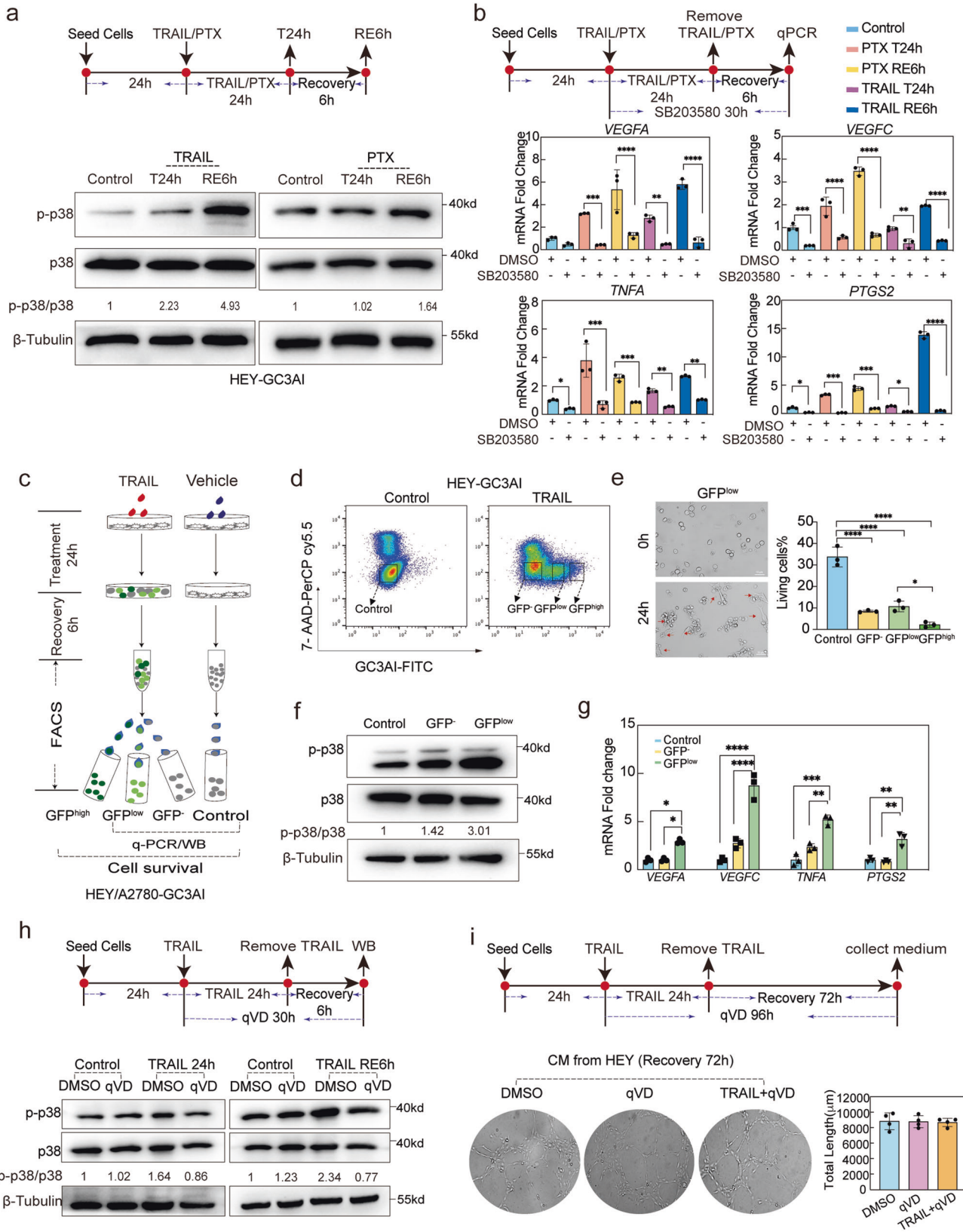


Fig. 6 The enhanced angiogenic capacity in the anastatic HEY cells depends on elevated p38 activity. **a** Western blots of the indicated phosphorylated proteins and total proteins in all the populations established from HEY cells. The numbers below each pair of the blots are the normalized ratios of the band intensity. **b** The mRNA expression of *VEGFA*, *VEGFC*, *TNFA* and *PTGS2* in the indicated populations with or without 24 h treatment of the p38 inhibitor SB203580. $n = 3$. 0.1% DMSO was used as control for SB203580. **c**, **d** The tube formation of HUVECs triggered by the conditioned medium (CM) collected from the indicated populations treated with or without SB203580 for 24 h. $n = 3$. **e**, **f** The tube formation of HUVECs triggered by CM collected from the indicated populations transfected with siNC (control) or siMAPK14#1 for 48 h. $n = 3$. **g**, **h** The results of Matrigel implant assays to show the in vivo angiogenesis triggered by CM from the indicated populations. On the left are the representative images of the Matrigel implants and on the right are the quantifications of Hemoglobin content in the Matrigel implants. $n = 4$. **i**, **j** The representative images of CD31 staining in the sections of the Matrigel implants. The scale bar is 20 μm . Data are presented as the mean \pm SEM. * $P < 0.05$; ** $P < 0.01$; *** $P < 0.001$; **** $P < 0.0001$.



the control populations had detectable caspase-3 activity (Supplementary Fig. S8a). Moreover, the upregulated expression of pro-angiogenic genes in the ZsGreen⁺ populations was not attenuated by qVD (Supplementary Fig. S8b), suggesting the pro-

angiogenic phenotypes of the anastatic cells are not due to any residual executioner caspase activity. The KEGG pathway analysis revealed enrichment of the DEGs in TNFR signaling pathway (Fig. 2e, Supplementary Fig. S2d). The kinases downstream of

Fig. 7 p38 is activated by caspases during apoptosis induction and early recovery. **a** Western blots of phosphor-p38 and p38 in HEY cells treated with TRAIL (TRAIL T24h), PTX (PTX T24h) or control for 24 h and in HEY cells after 6 h recovery from TRAIL or PTX treatment (TRAIL RE6h or PTX RE6h). The numbers below the blots are the normalized ratios of the band intensity. **b** The mRNA expression of *VEGFA*, *VEGFC*, *TNFA*, and *PTGS2* in control HEY cells, HEY cells treated with PTX or TRAIL for 24 h and cells after 6 h recovery from PTX or TRAIL treatment with or without the presence of the p38 inhibitor SB203580. $n = 3$. 0.1% DMSO was used as control for SB203580. **c** The schematic of cell treatment and sorting. WB Western Blotting. **d** The representative of flow cytometry showing isolation of GFP⁺, GFP^{low} and GFP^{high} populations from TRAIL-treated HEY-GC3AI cells and isolation of control population. **e** The percentage of living cells at 24 h after cell sorting in the indicated groups. Red arrows in the left images point to attached living cells. $n = 3$. **f** Western blots showing p38 phosphorylation in the indicated groups. **g** RT-qPCR results showing expression of *VEGFA*, *VEGFC*, *TNFA*, *PTGS2* in the indicated groups. $n = 3$. **h** Western blots showing the effect of qVD on p38 phosphorylation after 24 h TRAIL treatment (TRAIL 24 h) and after 6 h recovery (RE6h). 0.1% DMSO was used as control for qVD. **i** Tube formation assays of HUVECs incubated with conditioned medium (CM) from HEY-GC3AI cells treated with 0.1% DMSO, 50 μ M qVD, or 400 ng/ml TRAIL + 50 μ M qVD as shown in the schematic. $n = 4$. Data are presented as the mean \pm SEM. * $P < 0.05$; ** $P < 0.01$; *** $P < 0.001$; **** $P < 0.0001$.

TNFR like MAPK, NF κ B and Akt have all been reported to regulate angiogenesis [25–32]. We evaluated the activity of JNK, ERK, p38, Akt and NF κ B in different cell populations. Only p38 was found to be activated in all of the ZsGreen⁺ populations compared to the counterpart ZsGreen⁻ populations or the control populations (Fig. 6a, Supplementary Fig. S9a). We then tested the effect of inhibiting different pathways on the pro-angiogenic capacity of the anastatic cells. Among the tested inhibitors, only p38 inhibitor suppressed upregulation of all four pro-angiogenic genes in all the ZsGreen⁺ populations (Fig. 6b, Supplementary Figs. S9b, S10, S11). Moreover, treating different populations of the cancer cells with inhibitors for p38 but not the other kinases abolished the difference in their capacity to trigger tube formation of HUVECs (Fig. 6c, d, Supplementary Figs. S9c, d and S12). Suppression of enhanced pro-angiogenic capacity in the ZsGreen⁺ populations were also achieved using two independent siRNAs against *MAPK14* gene, which encodes p38 α (Fig. 6e, f, Supplementary Figs. S9e, f, S13, S14). Suppression of p38 in cancer cells also prevented upregulation in the in vivo angiogenic capacity of the conditioned medium from ZsGreen⁺ populations (Fig. 6g–j, Supplementary Fig. S9g–j). These data suggest that increased pro-angiogenic capacity in the anastatic cells relies on elevated p38 activity.

We also evaluated whether the kinases in TNFR signaling are involved in the enhanced migration of anastatic cells. While inhibition of Akt had no effect on migration, inhibition of either p38, JNK, NF κ B or ERK reduced the difference in migration between the ZsGreen⁺ cells and the other two types of cells (Supplementary Figs. S15 and S16), suggesting the enhanced migration of anastatic cells requires activity of multiple kinases.

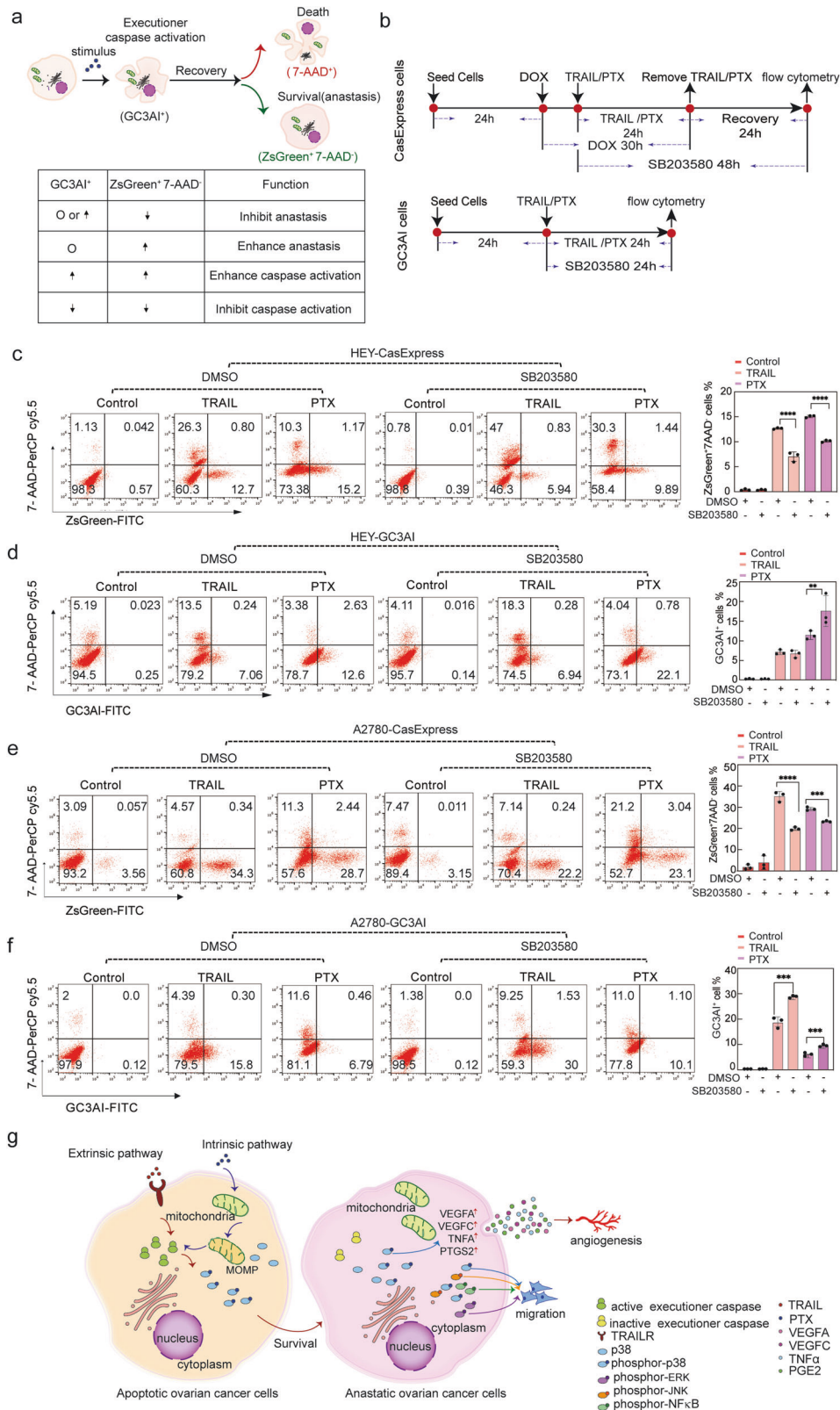
p38 is activated by caspases during apoptosis induction and early recovery

As a major stress response kinase, p38 is known to be activated in response to a wide variety of stimuli [33, 34]. We monitored p38 activity in cancer cells during their exposure to apoptotic stimuli and the early recovery phase. Increased phosphor-p38 was indeed detected in HEY cells at the end of 24 h TRAIL treatment and in A2780 cells at the end of 24 h treatment with TRAIL or PTX. Interestingly, the phosphor-p38 level was even further upregulated at the recovery phase (Fig. 7a, Supplementary Fig. S17a). Although the phosphor-p38 remained unchanged in HEY cells after 24 h PTX treatment, it was elevated after 6 h recovery (Fig. 7a). We also observed upregulation of the pro-angiogenic genes in HEY and A2780 cells at 6 h recovery after treatment, which was suppressed by p38 inhibition (Fig. 7b, Supplementary Fig. S17b). These results suggest that activation of p38 and the p38-dependent induction of pro-angiogenic gene expression were initiated during treatment, increased during early recovery and persisted after cells were fully recovered. To investigate whether p38 activation during treatment and early recovery is related to caspase activation, we isolated cells with different levels of GFP intensity (GFP⁺, GFP^{low} and GFP^{high}) from HEY-GC3AI and

A2780-GC3AI cells at 6 h recovery from TRAIL treatment (Fig. 7c, d, Supplementary Fig. S17c). At 24 h after sorting, the percentage of living cells was similar in the GFP^{low} populations and in the GFP^{high} populations but strongly reduced in the GFP^{high} populations (Fig. 7e, Supplementary Fig. S17d), suggesting the “live or die” fate after executioner caspase activation may be determined by the level of executioner caspase activity. We further compared p38 activity and expression of pro-angiogenic genes in the GFP^{low} populations, to those in the GFP^{high} populations. Both p38 activation and expression of pro-angiogenic genes were dramatically upregulated in the GFP^{low} populations (Fig. 7f, g, Supplementary Fig. S17e, f). Furthermore, inhibition of caspase activity suppressed p38 activation and expression of pro-angiogenic genes at the end of 24 h TRAIL treatment and after 6 h recovery (Fig. 7h, Supplementary Figs. S17g and S18a–d), indicating p38 activation and the p38-dependent expression of pro-angiogenic genes during treatment and early recovery relies on caspase activity. Moreover, cancer cells with caspases inhibited during TRAIL treatment and the first 72 h recovery displayed migration and pro-angiogenic capacity similar to those without TRAIL treatment (Fig. 7i, Supplementary Figs. S17h and S18e, f), suggesting the TRAIL-induced upregulation of migration and pro-angiogenic capacity relies on caspases. In addition, treatment with dehydrocorydaline, which induced p38 activation independent of caspases, was sufficient to increase the migration and pro-angiogenic capacity of HEY or A2780 cells (Supplementary Fig. S19). These data together indicate that stress-induced executioner caspase activation triggers p38 activation, which persist to confer anastatic cells enhanced migration and pro-angiogenic capacity.

p38 activation during apoptosis induction and recovery is required for anastasis

p38 is a stress-activated kinase that can promote both apoptosis and survival [33, 34]. We then investigated whether p38 activation during treatment and recovery is required for anastasis. We developed a strategy to evaluate the effects of various chemicals on anastasis using the GC3AI and the mCasExpress reporters. Upon treatment with apoptosis stimuli, cells with activated executioner caspases either die or undergo anastasis and survive. A reduction in the percentage of cells that survive executioner caspase activation (ZsGreen⁺ 7-AAD⁻), but not the percentage of cells with executioner caspase activation (GC3AI⁺), would indicate inhibition of anastasis. On the other hand, an increase in the percentage of ZsGreen⁺ 7-AAD⁻ cells, but not the percentage of GC3AI⁺ cells, would indicate enhancement of anastasis (Fig. 8a). p38 inhibition by SB203580 reduced the fraction of ZsGreen⁺ 7-AAD⁻ cells in HEY-CasExpress cells recovered from TRAIL or PTX treatment (Fig. 8b, c) while the percentage of TRAIL- or PTX-induced GC3AI⁺ HEY cells remained unchanged or increased (Fig. 8b, d). Similar results were obtained in A2780 cells (Fig. 8e, f). These data indicate that anastasis in ovarian cancer cells following TRAIL or PTX treatment requires p38 activity.



DISCUSSION

The discovery of anastasis unveils two types of apoptotic resistance, avoidance of executioner caspase activation and anastasis, both of which spare cells from apoptotic death. In this

study, we aim to characterize the differences between ovarian cancer cells that survive through these two distinct types of apoptotic resistance and to investigate the underlying mechanism. We demonstrate that in ovarian cancer cells facing apoptotic

Fig. 8 p38 activation during apoptosis induction and recovery is required for anastasis. **a** The schematic of the strategy to analyze the effect of a chemical on anastasis or caspase activation. "O" indicates no change. **b** The schematic showing the procedure for cell treatment. **c** Representative images and quantification of flow cytometry showing the percentage of ZsGreen⁺ 7-AAD⁻ cells in HEY-CasExpress cells after 24 h recovery from TRAIL or PTX treatment with or without SB203580. 0.1% DMSO was used as control for SB203580. **d** Representative images and quantification of flow cytometry showing the percentage of GC3AI⁺ cells in HEY-GC3AI cells after 24 h treatment with TRAIL or PTX with or without SB203580. **e** Representative images and quantification of flow cytometry showing the percentage of ZsGreen⁺ 7-AAD⁻ cells in A2780-CasExpress cells after 24 h recovery from TRAIL or PTX treatment with or without SB203580. **f** Representative images and quantification of flow cytometry showing the percentage of GC3AI⁺ cells in A2780-GC3AI cells after 24 h treatment with TRAIL or PTX with or without SB203580. $n = 3$. Data are presented as the mean \pm SEM. * $P < 0.05$; ** $P < 0.01$; *** $P < 0.001$; **** $P < 0.0001$. **g** Summary of the molecular events during and after anastasis. In ovarian cancer cells facing apoptotic stress, active executioner caspase induces p38 activation to promote anastasis. The elevated p38 activation persists in anastatic cells to drive migration together with ERK, JNK and NF κ B and to promote angiogenesis, leading to enhanced tumor angiogenesis, growth and metastasis.

stress, the active executioner caspases induce p38 activation to promote anastasis, and that the elevated p38 activity persists in the anastatic cells to drive migration and the expression of pro-angiogenic genes, leading to enhanced tumor angiogenesis, growth and metastasis (Fig. 8g).

We found that ovarian cancer cells gained enhanced migration after survival from executioner caspase activation. Similar observation has also been reported in breast cancer cells, cervical cancer cells, and melanoma [5, 7, 9], indicating that migration enhancement is a common phenotypic change accompanying anastasis. More importantly, we demonstrated that anastatic cancer cells are more pro-angiogenic. It has been reported that apoptotic glioma cells and breast cancer cells can trigger angiogenesis through caspase-dependent secretion of pro-angiogenic factors like VEGFA and PGE2 [23, 24]. Previously, we and others demonstrated upregulated expression of pro-angiogenic genes in HeLa cells [5] and in primary mouse liver cells [35] within 24 h recovery from ethanol treatment. Consistently, here we observed elevated expression of pro-angiogenic factors at 6 h after removal of apoptotic stimuli. We further showed that cells with executioner caspase activation exhibited higher expression of pro-angiogenic genes than those without executioner caspase activation and that inhibition of caspases during exposure to apoptosis stimuli and recovery blocked the afterward enhancement in the capacity of the cancer cells to promote angiogenesis. These data together indicate that stress-induced executioner caspase activation is essential for anastatic cells to become more angiogenic. Interestingly, the anastatic cells remained more angiogenic even when they were separated from dead cells and no longer had caspase activity, suggesting that although caspase activity is necessary for initiating the change in angiogenesis, neither the presence of apoptotic cells nor active executioner caspases is required for anastatic cells to maintain a high pro-angiogenic capacity.

How do anastatic cells maintain enhanced pro-angiogenic capacity when they no longer have executioner caspase activity? Two possible mechanisms may be involved. First, consistent with previous reports [26, 27, 31, 36–38], we found the increased expression of pro-angiogenic genes in anastatic cells relied on p38 activity. In the meanwhile, pro-angiogenic factors like VEGFs and TNF α can also activate p38 [39–42]. Therefore, p38 and the pro-angiogenic factors may form a positive feedback loop to maintain the high p38 activity and strong expression of pro-angiogenic genes in anastatic cells. On the other hand, in mouse brain exposed to ethanol, caspase-3 activation has been shown to induce epigenetic changes through degradation of DNA methyltransferases DNMT1 and DNMT3A and methyl-CpG binding protein MeCP2 [43, 44]. Therefore, transient executioner caspase activation may induce epigenetic changes in anastatic cells, leading to persisting expression of p38 activators. Further investigation is needed to unveil the underlying mechanism.

It is important to elucidate the factors that regulate anastasis. We previously identified two essential drivers for anastasis, Akt1 and Ciz1, in *Drosophila* [10]. Seervi et al. found inhibition of XPO1, a key molecule in the nuclear export pathway, suppresses anastasis in breast cancer cells after exposure to chemotherapeutic drugs [7]. Here we identified p38 as a key regulator of anastasis in ovarian cancer cells. As a stress-activated kinase, the pro-apoptotic role of p38 is well established. Activated p38 can trigger apoptosis through phosphorylation of Bim, Bax and p53 [45–47]. However, p38 has also been reported to have pro-survival function. Inhibition of p38 sensitizes cancer cells to radiation- or chemotherapy-induced apoptosis [48–51]. Active p38 can promote survival through activation of β -catenin [52] and JAK/STAT signaling [53]. p38 activation also causes G1 arrest and cellular senescence, which can be regarded as survival strategies to resist apoptosis in some cell types [45, 54–56]. Our work reveals that p38 promotes anastasis, survival after stress-induced executioner caspase activation. How does p38 regulate anastasis? Valon et al. reported that the pulse of ERK activity in cells with mild executioner caspase activation blocks accumulation of executioner caspase activity and protects the cells from death in *Drosophila* notum epithelium [57], suggesting interrupting amplification of executioner caspase activity may be a way to promote anastasis. Alvarado-Kristensson et al. found p38 can phosphorylate caspase-8 and caspase-3 to inhibit their protease activity in isolated neutrophils [58]. Therefore, in cancer cells facing apoptotic stress, p38 activation induced by active executioner caspases may in turn block further amplification of executioner caspase activity, leading to anastasis. Further efforts are needed to test this hypothesis.

In conclusion, our work demonstrates that anastatic cancer cells become more malignant via their enhanced migratory and pro-angiogenic capacities. These newly acquired features enable them to invade more aggressively and to create a pro-tumor microenvironment. Targeting anastasis during chemotherapy may prevent tumor relapse and metastasis.

DATA AVAILABILITY

The raw data for RNAseq can be assessed at PRJNA798831. All the other raw data supporting the findings of this study are available from the corresponding author upon request. Original Western blots are provided with this paper.

REFERENCES

1. Ichim G, Tait SW. A fate worse than death: apoptosis as an oncogenic process. *Nat Rev Cancer*. 2016;16:539–48.
2. Green D, Kroemer G. The central executioners of apoptosis: caspases or mitochondria? *Trends Cell Biol*. 1998;8:267–71.
3. Sun G, Montell DJ. Q&A: Cellular near death experiences-what is anastasis? *BMC Biol*. 2017;15:92.
4. Tang HM, Tang HL. Anastasis: recovery from the brink of cell death. *R Soc Open Sci*. 2018;5:180442.

5. Sun G, Guzman E, Balasanyan V, Conner CM, Wong K, Zhou HR, et al. A molecular signature for anastasis, recovery from the brink of apoptotic cell death. *J Cell Biol.* 2017;216:3355–68.
6. Tang HL, Tang HM, Mak KH, Hu S, Wang SS, Wong KM, et al. Cell survival, DNA damage, and oncogenic transformation after a transient and reversible apoptotic response. *Mol Biol Cell.* 2012;23:2240–52.
7. Seervi M, Sumi S, Chandrasekharan A, Sharma AK, SanthoshKumar TR. Molecular profiling of anastatic cancer cells: potential role of the nuclear export pathway. *Cell Oncol.* 2019;42:645–61.
8. Xu Y, So C, Lam HM, Fung MC, Tsang SY. Apoptosis reversal promotes cancer stem cell-like cell formation. *Neoplasia.* 2018;20:295–303.
9. Berthenet K, Castillo Ferrer C, Fanfone D, Popgeorgiev N, Neves D, Bertolino P, et al. Failed apoptosis enhances melanoma cancer cell aggressiveness. *Cell Rep.* 2020;31:107731.
10. Sun G, Ding XA, Argaw Y, Guo X, Montell DJ. Akt1 and dCIZ1 promote cell survival from apoptotic caspase activation during regeneration and oncogenic overgrowth. *Nat Commun.* 2020;11:5726.
11. Liu X, He Y, Li F, Huang Q, Kato TA, Hall RP, et al. Caspase-3 promotes genetic instability and carcinogenesis. *Mol Cell.* 2015;58:284–96.
12. Cartwright IM, Liu X, Zhou M, Li F, Li CY. Essential roles of Caspase-3 in facilitating Myc-induced genetic instability and carcinogenesis. *Elife.* 2017;6:e26371.
13. Carneiro BA, El-Deiry WS. Targeting apoptosis in cancer therapy. *Nat Rev Clin Oncol.* 2020;17:395–417.
14. Naresh KN, Lakshminarayanan K, Pai SA, Borges AM. Apoptosis index is a predictor of metastatic phenotype in patients with early stage squamous carcinoma of the tongue: a hypothesis to support this paradoxical association. *Cancer* 2001;91:578–84.
15. Isobe N, Onodera H, Mori A, Shimada Y, Yang W, Yasuda S, et al. Caspase-3 expression in human gastric carcinoma and its clinical significance. *Oncology* 2004;66:201–9.
16. Hu Q, Peng J, Liu W, He X, Cui L, Chen X, et al. Elevated cleaved caspase-3 is associated with shortened overall survival in several cancer types. *Int J Clin Exp Pathol.* 2014;7:5057–70.
17. Zhang Z, Wang M, Zhou L, Feng X, Cheng J, Yu Y, et al. Increased HMGB1 and cleaved caspase-3 stimulate the proliferation of tumor cells and are correlated with the poor prognosis in colorectal cancer. *J Exp Clin Cancer Res.* 2015;34:51.
18. Ford CA, Petrova S, Pound JD, Voss JJ, Melville L, Paterson M, et al. Oncogenic properties of apoptotic tumor cells in aggressive B cell lymphoma. *Curr Biol.* 2015;25:577–88.
19. Zhao R, Kaakati R, Lee AK, Liu X, Li F, Li CY. Novel roles of apoptotic caspases in tumor repopulation, epigenetic reprogramming, carcinogenesis, and beyond. *Cancer Metastasis Rev.* 2018;37:227–36.
20. Yang X, Zhong DN, Qin H, Wu PR, Wei KL, Chen G, et al. Caspase-3 overexpression is associated with poor overall survival and clinicopathological parameters in breast cancer: a meta-analysis of 3091 cases. *Oncotarget* 2018;9:8629–41.
21. Zhang J, Wang X, Cui W, Wang W, Zhang H, Liu L, et al. Visualization of caspase-3-like activity in cells using a genetically encoded fluorescent biosensor activated by protein cleavage. *Nat Commun.* 2013;4:2157.
22. Ding AX, Sun G, Argaw YG, Wong JO, Easwaran S, Montell DJ. CasExpress reveals widespread and diverse patterns of cell survival of caspase-3 activation during development in vivo. *Elife.* 2016;5:e10936.
23. Feng X, Yu Y, He S, Cheng J, Gong Y, Zhang Z, et al. Dying glioma cells establish a proangiogenic microenvironment through a caspase 3 dependent mechanism. *Cancer Lett.* 2017;385:12–20.
24. Bernard A, Chevrier S, Beltjens F, Dosset M, Viltard E, Lagrange A, et al. Cleaved caspase-3 transcriptionally regulates angiogenesis-promoting chemotherapy resistance. *Cancer Res.* 2019;79:5958–70.
25. Mudgett JS, Ding J, Guh-Siesel L, Chartrain NA, Yang L, Gopal S, et al. Essential role for p38alpha mitogen-activated protein kinase in placental angiogenesis. *Proc Natl Acad Sci USA.* 2000;97:10454–9.
26. Gonzalez-Villasana V, Fuentes-Mattei E, Ivan C, Dalton HJ, Rodriguez-Aguayo C, Fernandez-de Thomas RJ, et al. Rac1/Pak1/p38/MMP-2 axis regulates angiogenesis in ovarian cancer. *Clin Cancer Res.* 2015;21:2127–37.
27. Varinska L, Gal P, Mojzisova G, Mirossay L, Mojzis J. Soy and breast cancer: focus on angiogenesis. *Int J Mol Sci.* 2015;16:11728–49.
28. Patel M, Horgan PG, McMillan DC, Edwards J. NF-kappaB pathways in the development and progression of colorectal cancer. *Transl Res.* 2018;197:43–56.
29. Revathidevi S, Munirajan AK. Akt in cancer: mediator and more. *Semin Cancer Biol.* 2019;59:80–91.
30. Guo YJ, Pan WW, Liu SB, Shen ZF, Xu Y, Hu LL. ERK/MAPK signalling pathway and tumorigenesis. *Exp Ther Med.* 2020;19:1997–2007.
31. Harry JA, Ormiston ML. Novel pathways for targeting tumor angiogenesis in metastatic breast cancer. *Front Oncol.* 2021;11:772305.
32. Tam SY, Law HK. JNK in tumor microenvironment: present findings and challenges in clinical translation. *Cancers.* 2021;13:2196.
33. Han J, Wu J, Silke J. An overview of mammalian p38 mitogen-activated protein kinases, central regulators of cell stress and receptor signaling. *F1000Res.* 2020;9:F1000 Faculty Rev-653.
34. Martinez-Limon A, Joaquin M, Caballero M, Posas F, de Nadal E. The p38 pathway: from biology to cancer therapy. *Int J Mol Sci.* 2020;21:1913.
35. Tang HM, Talbot CC Jr, Fung MC, Tang HL. Molecular signature of anastasis for reversal of apoptosis. *F1000Res.* 2017;6:43.
36. Xu K, Shu HK. EGFR activation results in enhanced cyclooxygenase-2 expression through p38 mitogen-activated protein kinase-dependent activation of the Sp1/Sp3 transcription factors in human gliomas. *Cancer Res.* 2007;67:6121–9.
37. Leelahavanichkul K, Amornphimoltham P, Molinolo AA, Basile JR, Koontongkaew S, Gutkind JS. A role for p38 MAPK in head and neck cancer cell growth and tumor-induced angiogenesis and lymphangiogenesis. *Mol Oncol.* 2014;8:105–18.
38. Limoge M, Safina A, Truskinovsky AM, Aljhdali I, Zonneville J, Gruevski A, et al. Tumor p38MAPK signaling enhances breast carcinoma vascularization and growth by promoting expression and deposition of pro-tumorigenic factors. *Oncotarget.* 2017;8:61969–81.
39. Rousseau S, Houle F, Landry J, Huot J. p38 MAP kinase activation by vascular endothelial growth factor mediates actin reorganization and cell migration in human endothelial cells. *Oncogene.* 1997;15:2169–77.
40. Li YP, Chen Y, John J, Moylan J, Jin B, Mann DL, et al. TNF-alpha acts via p38 MAPK to stimulate expression of the ubiquitin ligase atrogin1/MAFbx in skeletal muscle. *FASEB J.* 2005;19:362–70.
41. Wu G, Luo J, Rana JS, Laham R, Sellke FW, Li J. Involvement of COX-2 in VEGF-induced angiogenesis via P38 and JNK pathways in vascular endothelial cells. *Cardiovasc Res.* 2006;69:512–9.
42. Zhou FH, Foster BK, Zhou XF, Cowin AJ, Xian CJ. TNF-alpha mediates p38 MAP kinase activation and negatively regulates bone formation at the injured growth plate in rats. *J Bone Min Res.* 2006;21:1075–88.
43. Nagre NN, Subbanna S, Shivakumar M, Psychoyos D, Basavarajappa BS. CB1-receptor knockout neonatal mice are protected against ethanol-induced impairments of DNMT1, DNMT3A, and DNA methylation. *J Neurochem.* 2015;132:429–42.
44. Subbanna S, Nagre NN, Shivakumar M, Joshi V, Psychoyos D, Kutlar A, et al. CB1R-mediated activation of caspase-3 causes epigenetic and neurobehavioral abnormalities in postnatal ethanol-exposed mice. *Front Mol Neurosci.* 2018;11:45.
45. Kishi H, Nakagawa K, Matsumoto M, Suga M, Ando M, Taya Y, et al. Osmotic shock induces G1 arrest through p53 phosphorylation at Ser33 by activated p38MAPK without phosphorylation at Ser15 and Ser20. *J Biol Chem.* 2001;276:39115–22.
46. Cai B, Chang SH, Becker EB, Bonni A, Xia Z. p38 MAP kinase mediates apoptosis through phosphorylation of BimEL at Ser-65. *J Biol Chem.* 2006;281:25215–22.
47. Min H, Ghatnekar GS, Ghatnekar AV, You X, Bu M, Guo X, et al. 2-Methoxyestradiol induced Bax phosphorylation and apoptosis in human retinoblastoma cells via p38 MAPK activation. *Mol Carcinog.* 2012;51:576–85.
48. Canovas B, Igea A, Sartori AA, Gomis RR, Paull TT, Isoda M, et al. Targeting p38alpha increases DNA damage, chromosome instability, and the anti-tumoral response to taxanes in breast cancer cells. *Cancer Cell.* 2018;33:1094–110.e8.
49. Garcia-Cano J, Roche O, Cimas FJ, Pascual-Serra R, Ortega-Muelas M, Fernandez-Aroca DM, et al. p38MAPK and chemotherapy: we always need to hear both sides of the story. *Front Cell Dev Biol.* 2016;4:69.
50. Pereira L, Igea A, Canovas B, Dolado I, Nebreda AR. Inhibition of p38 MAPK sensitizes tumour cells to cisplatin-induced apoptosis mediated by reactive oxygen species and JNK. *EMBO Mol Med.* 2013;5:1759–74.
51. Yang SY, Miah A, Sales KM, Fuller B, Seifalian AM, Winslet M. Inhibition of the p38 MAPK pathway sensitises human colon cancer cells to 5-fluorouracil treatment. *Int J Oncol.* 2011;38:1695–702.
52. Thornton TM, Pedraza-Alva G, Deng B, Wood CD, Aronshtam A, Clements JL, et al. Phosphorylation by p38 MAPK as an alternative pathway for GSK3beta inactivation. *Science.* 2008;320:667–70.
53. Santabarbara-Ruiz P, Lopez-Santillan M, Martinez-Rodriguez I, Binagui-Casas A, Perez L, Milan M, et al. ROS-induced JNK and p38 signaling is required for unpaired cytokine activation during drosophila regeneration. *PLoS Genet.* 2015;11:e1005595.
54. Guo H, Liu Z, Xu B, Hu H, Wei Z, Liu Q, et al. Chemokine receptor CXCR2 is transactivated by p53 and induces p38-mediated cellular senescence in response to DNA damage. *Aging Cell.* 2013;12:1110–21.
55. Zhang X, Liu Z, Xu B, Sun Z, Gong Y, Shao C. Neferine, an alkaloid ingredient in lotus seed embryo, inhibits proliferation of human osteosarcoma cells by promoting p38 MAPK-mediated p21 stabilization. *Eur J Pharm.* 2012;677:47–54.
56. Lafarga V, Cuadrado A, Lopez de Silanes I, Bengoechea R, Fernandez-Capetillo O, Nebreda AR. p38 Mitogen-activated protein kinase- and HuR-dependent stabilization of p21(Cip1) mRNA mediates the G(1)/S checkpoint. *Mol Cell Biol.* 2009;29:4341–51.

57. Valon L, Davidovic A, Levillayer F, Villars A, Chouly M, Cerqueira-Campos F, et al. Robustness of epithelial sealing is an emerging property of local ERK feedback driven by cell elimination. *Dev Cell*. 2021;56:1700–11.e8.
58. Alvarado-Kristensson M, Melander F, Leandersson K, Ronnstrand L, Wernstedt C, Andersson T. p38-MAPK signals survival by phosphorylation of caspase-8 and caspase-3 in human neutrophils. *J Exp Med*. 2004;199:449–58.

ACKNOWLEDGEMENTS

We thank Translational Medicine Core Facility of Shandong University for technical support.

AUTHOR CONTRIBUTIONS

GS and LS designed the experiments. LS, YC, XL, YW, and RW carried out the experiments. GS, LS, DJM, CS, YG, MW, and QL prepared the manuscript.

FUNDING

This work was supported by National Natural Science Foundation of China (No. 31970781 and 81902837), Rongxiang Regenerative Medicine Foundation of Shandong University (No. 2019SDRX-06) and the Funds for Youth Interdisciplinary and Innovation Research Group of Shandong University (2020QNQT003) to GS.

COMPETING INTERESTS

The authors declare no competing interests.

ETHICS APPROVAL

The research was approved by the Animal Care and Use Committee of Shandong University.

ADDITIONAL INFORMATION

Supplementary information The online version contains supplementary material available at <https://doi.org/10.1038/s41418-022-01081-1>.

Correspondence and requests for materials should be addressed to Gongping Sun.

Reprints and permission information is available at <http://www.nature.com/reprints>

Publisher's note Springer Nature remains neutral with regard to jurisdictional claims in published maps and institutional affiliations.

Springer Nature or its licensor (e.g. a society or other partner) holds exclusive rights to this article under a publishing agreement with the author(s) or other rightsholder(s); author self-archiving of the accepted manuscript version of this article is solely governed by the terms of such publishing agreement and applicable law.